Analytical and Bioanalytical Chemistry
https://doi.org/10.1007/s00216-018-1341-y

RESEARCH PAPER

Graphene quantum dots-based nano-biointerface platform for food toxin detection

Hema Bhardwaj [1,2] · Chandan Singh [2] · R. K. Kotnala [2] · Gajjala Sumana [2]

Received: 18 April 2018 / Revised: 19 August 2018 / Accepted: 22 August 2018

Abstract

Due to the similar electrochemical properties to graphene oxide (GO), graphene quantum dots (GQDs) are considered as a highly potential candidate for designing an electrochemical biosensor. In this report, GQDs were synthesized having an average diameter of 7 nm and utilized for the fabrication of an electrochemical immunosensor for the detection of food toxin, aflatoxin B_1 (AFB_1). An electrophoretic deposition technique was utilized to deposit the chemically synthesized GQDs onto indium tin oxide (ITO)-coated glass substrate. Further, the monoclonal antibodies of AFB_1 were covalently immobilized onto deposited electrode GQDs/ITO using EDC-NHS as a crosslinker. The structural and morphological studies of GQDs and conjugated anti-AFB_1 with GQDs have been investigated using UV-visible spectroscopy, photoluminescence spectroscopy, Raman spectroscopy, transmission electron microscopy, scanning electron microscopy techniques, etc. The electrochemical impedance spectroscopy and cyclic voltammetry measurements were carried out for electrical characterization and biosensing studies. This simple monodisperse GQDs-based platform yields heterogeneous electron transfer (97.63×10^{-5} cm s^{-1}), the time constant (0.005 s) resulting in improved biosensing performance. The electrochemical immunosensor shows high sensitivity 213.88 Ω (ng $mL^{-1})^{-1}$ cm^{-2}. The limit of detection for standard samples and contaminated maize samples was found to be 0.03 ng mL^{-1} and 0.05 ng g^{-1}, respectively, which is lower than the maximum acceptable limit according to the European Union. This result indicates its potential application for aflatoxin B_1 detection in food contents.

Keywords Graphene quantum dots · Electrophoretic deposition · Aflatoxin B_1 · Electrochemical immunosensor · Impedance

Introduction

Aflatoxins are a naturally occurring secondary metabolite produced by A*spergillus flavus* and A*spergillus parasiticus* [1]. There are mainly four groups of aflatoxins, namely B_1, B_2, G_1, and G_2, among which AFB_1 is a highly toxic furano-coumarin derivative of double furan ring and coumarin moiety chemical product which is responsible for liver cancer [2]. AFB_1 is mostly found in the daily usage of food products like maize, groundnut, corn, cereals, rice, pistachio, wheat, species, etc. AFB_1 is classified as a group I carcinogenic compound according to the International Agency for Research on Cancer (IARC) [3]. The European Commission has set the maximum permissible limit of aflatoxin B_1 4 μg kg^{-1} and content of total aflatoxins in food products are 10 μg kg^{-1} [4]. Although, some conventional techniques are available to detect the aflatoxin B_1 such as thin layer chromatography (TLC), high-performance liquid chromatography (HPLC), liquid chromatography combined with mass spectroscopy (LC-MS) and so on. However, these techniques are expensive and time-consuming with complex handling procedure and require highly skilled personnel [5]. Thus, to overcome these drawbacks, there is an urgent need for rapid, accurate, and specific detecting tool to determine the content of aflatoxins in food products. Hence, the electrochemical biosensor could be one of the most suitable, sensitive, simple, and alternate tool which may ensure the safety of daily usage of food products.

Electronic supplementary material The online version of this article (https://doi.org/10.1007/s00216-018-1341-y) contains supplementary material, which is available to authorized users.

✉ Gajjala Sumana
sumanagajjala@gmail.com

[1] Academy of Scientific and Innovative Research, CSIR-National Physical Laboratory, Dr. K.S.Krishnan Marg, New Delhi 110012, India

[2] CSIR-National Physical Laboratory, Dr. K.S.Krishnan Marg, New Delhi 110012, India

Published online: 14 September 2018

The carbon-based materials such as GO, fullerenes, graphene sheets, GQDs commonly used as a remarkable nanomaterial for the bioanalytical field, owing to their inherent properties such as biocompatible, structural flexibility, ease of synthesis, etc. [6]. Moreover, graphene is one of the widely used nanomaterials in the field of biosensor because of their attractive properties such as the large surface area, high charge carrier mobility, and mechanical flexibility [7]. Although, graphene is zero-band gap material and their sheets are not easily dispersed in an aqueous medium. However, the band gap of the nanomaterials can be altered by altering the size, shape, thickness, and fraction of SP^2 domain behavior. Thus, reducing the size of graphene sheets in the smaller nanoscale region perhaps leads to change the several desirable properties especially optical and electronic properties. The GQDs are nanocrystals belonging to a nanometer scale with a lateral dimension less than 100 nm having single to few layers of graphene sheets in a tiny dot structure which shows their tremendous interest in the biosensing and bioimaging research field, owing to their remarkable properties such as low toxicity, photostability, biocompatibility, wide absorption, narrow emission band spectra, low reactivity, and dispersibility [8]. The presence of hydrophobic edges as well as hydrophilic planes in GQDs and a large surface to volume ratio as well as a favorable electron donor and acceptor ability tend to improve the adsorption capability for biomolecules upon the electrode surface and enhance the electrochemical signal [9]. For example, Yang et al. demonstrated the application for tumor marker detection using nanocomposite and GQDs, leading to enhance the electrical conductivity and surface area of the matrix [10]. Graphene quantum dots beads being utilized in an immunochromatographic assay for ultrasensitive detection of aflatoxin B_1 where the limit of detection found to be 0.42 pg mL^{-1} [11]. Moreover, Qian et al. have developed ultrasensitive DNA nanosensor based on fluorescence resonance energy transfer (FRET) phenomenon between biocompatible GQDs and carbon nanotubes (CNT), where the labeled probe of GQDs served as an electron donor property along with an electroluminescent behavior [12]. Zhang et al. developed the sensor for hydrogen peroxide (H_2O_2) detection using the GQDs/Au electrode where GQDs act as an electron transporter [13]. Moreover, Deng et al. demonstrate specific cell surface protein imaging based on the gold nanocube@silica@GQDs hybrid, where GQDs act as an electron transfer channel [14]. And, GQDs contain a lot of functional groups moieties such as carboxylic, hydroxyl, and epoxy at the edge planes that able to improve their dispersion ability in an aqueous medium. Various synthesis routes have been developed for the synthesis of GQDs, especially categorized in two ways as a top-down and bottom-up approach, but to obtain the stable, uniform shape and size of QDs, a top-down approach widely used [15]. In the previous reports, GQDs modified electrodes were fabricated simply by the drop-casting method or through crosslinkers. Casting method is not easy to get uniform coating and not well to control the desired thickness of the film. Moreover, materials from the electrode leached out due to the existence of weak interactions. Thus, to overcome these major disadvantages, an electrophoretic deposition (EPD) technique has been utilized to resolve the deposit problem. EPD is one of the most suitable deposition tool to obtain the desired thickness, uniformity, and smoothness of the film [13].

Herein, we have constructed the label-free electrochemical immunosensor using biocompatible GQDs nanomaterial to detect the AFB_1. The aim of this study was to exploit the synthesis of GQDs, the direct EPD of chemically synthesized GQDs onto the electrode surface to obtain the uniform shape, size, and surface morphology and to fabricate the label-free immunosensor with specificity, stability, and high sensitivity. To the best of our knowledge, this is the first time we are reporting electrophoretic deposit GQDs-based platform which is utilized for fabrication of electrochemical immunosensor for AFB_1 detection.

Experimental

Materials

Monoclonal antibodies of aflatoxin B_1 (anti-AFB_1) of mouse and antigen of aflatoxin B_1 (AFB_1) were procured from Sigma-Aldrich, India. Graphite powder flakes (45 μm, 99.99 wt%), sulfuric acid (H_2SO_4), nitric acid (HNO_3), ammonia (NH_3), magnesium nitrate hexahydrate ($Mg(NO_3)_2.6H_2O$), H_2O_2, potassium permanganate ($KMnO_4$) N-ethyl-N-(3-dimethylaminopropyl) carbodiimide (EDC), N-hydroxysuccinimide (NHS), bovine serum albumin (BSA), and all other chemicals were purchased from Sigma-Aldrich, India, and were used as received. Deionized water (Milli-Q, Millipore, 18.2 M Ω cm) was used for the preparation of buffers and aqueous solutions. BSA (1 mg mL^{-1}) and anti-AFB_1 solutions were prepared in (50 mM) phosphate buffer saline (PBS) pH 7.4.

Instruments

EPD (Bio-rad, model 200/2.0) has been used to deposit GQDs onto ITO-coated glass substrate. Structural analysis has been investigated by spectroscopic and diffraction techniques such as UV-visible spectrophotometer (Lambda 950, Perkin-Elmer), Photoluminescence spectrophotometer (PL, Jobin Yvon-Horiba, model 3–11), Raman spectrometer (HR800 LabRam, Horiba/Jobin-Yvon), X-ray diffractometer (Cu Kα radiation, Rigaku), Fourier Transform Infrared spectrometer (FT-IR, Spectrum BX, Perkin-Elmer), and transmission electron microscopy (TEM, Tecnaii-G2F30 STWIN). The morphology characterization has been done using scanning

electron microscopy technique (SEM, LEO440). The electrochemical studies such as electrochemical impedance spectroscopy (EIS) and cyclic voltammetry (CV) has been carried out using Autolab Galvanostat/Potentiostat (Eco Chemie, the Netherlands, model AUT84275) in phosphate-buffered saline (PBS, 50 mM, 0.9% NaCl, pH 7.4) containing mediator 5 mM $[Fe(CN)_6]^{3-/4-}$ in a three-electrode system where ITO was considered as the working electrode, Ag/AgCl as the reference electrode, and platinum act as the counter electrode.

Synthesis of graphene quantum dots

GO was synthesized using a modified Hummer's method with slight modification [16]. In brief, for pre-oxidation, graphite (1 g) and sodium nitrate (0.5 g) were mixed in 40 mL of concentrated H_2SO_4 under constant stirring. After 2 h, 3.5 g of $KMnO_4$ was added by keeping the temperature less than 20 °C. After that, the reaction mixture was continuously stirred at 35 °C for 12 h, then 10 mL of H_2O_2 (30%) was added dropwise. The resulting solution was washed with distilled water five times and dried in a vacuum oven at 80 °C. Further, GQDs were synthesized by prepared GO nanomaterials using the hydrothermal method [17]. In a 250-mL flask, 50 mg GO was dispersed in concentrated HNO_3 (30 mL) and concentrated H_2SO_4 (10 mL) and ultrasonicated (40 W, 0.25 A) for 15 h. The mixture was diluted with 200 mL of distilled water and filtered by a microporous membrane (0.22 μm) to remove the acids from the reaction mixture. The resulting suspension was dispersed in 40 mL of distilled water followed by adjusting the pH of the reaction mixture at 8.0 using 1 M sodium hydroxide. After that, the final solution was transferred in 50 mL Teflon-lined autoclave and heated at 200 °C for 10 h. After cooling at room temperature, the black suspension was filtered through a microporous membrane (0.22 μm), and the brown solution was separated out. Thus, the colloidal solution contained graphene sheets with some smaller molecules and ions. To improve the purity of GQDs, this colloidal solution was taken in a dialysis bag with a molecular weight of 1 KDa which was placed in an aqueous solution under constant stirring at room temperature for 3 days, and the dispersion medium was changed in every 15 h. Dissolved ions and small molecules are allowed to pass through this semi-permeable membrane which leads to improving the purity of GQDs. Thus, this colloidal solution as such remains in the dialysis tube while impurities get emerged out from it into the aqueous solution. The color of the solution changing from a brown solution to light brown yellow color indicates the purity of GQDs.

Electrophoretic deposition of graphene quantum dots

Schematic representation of synthesized GQDs, deposition and fabrication of immunosensor are depicted in Fig. 1. The synthesized GQDs are highly stable and uniformly dispersed in aqueous solution. The EPD technique was used to deposit GQDs onto ITO-coated glass electrode. Firstly, GQDs (1000 μL) of colloidal solution were dispersed in 10 mL distilled water and sonicated for 1 h at 30 °C to form a well-dispersed suspension followed by the addition of $Mg(NO_3)_2.6H_2O$ (10^{-4} to 10^{-5} mol). The $Mg(NO_3)_2.6H_2O$ has been used as an electrolyte to provide the positive charge onto the surface of GQDs where Mg^{2+} ions adsorbed by GQDs nanosheets [see Electronic Supplementary Material (ESM), Fig. S6]. Dispersed solution was taken in two electrode cells separated by 1 cm where platinum foil act as a cathode and hydrolyzed ITO-coated glass electrode (H_2O_2/NH_3/H_20; 1:1:5 ratio heated at 80 °C) act as an anode [18]. By applying the constant potential (5 V) to an ITO electrode

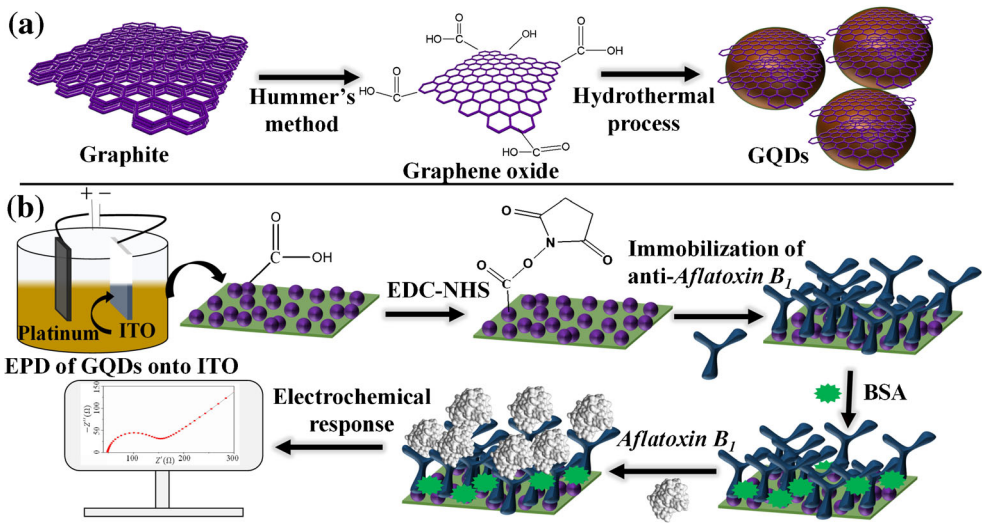

Fig. 1 Schematic representation (a) synthesis of GQDs from graphite and (b) EPD of GQDs onto ITO-coated glass substrate and immobilization of antibody using EDC-NHS chemistry followed by the AFB_1 detection

($0.5\ cm^2$, $20\ \Omega\ cm^{-1}$) for less than 1 min, GQDs easily deposited onto the ITO electrode substrate without disturbing their structure and surface morphology. Thus, the deposited electrode was removed from the suspension and then washed with distilled water several times and dried at room temperature. The chemically synthesized GQDs has negative zeta potential (− 10.0 mV) indicates the presence of various groups on the edge planes and basal planes. To obtain the well-ordered surface morphology with a uniform distribution over the electrode, certain parameters were optimized such as the concentration of $Mg(NO_3)_2.6H_2O$, time, and voltage.

Fabrication of BSA/anti-AFB_1/GQDs/ITO immunoelectrode

Before carrying out the immobilization process, the deposited electrode was activated by EDC-NHS coupling chemistry where EDC (0.2 M) was used as a coupling agent, and NHS (0.05 M) acted as an activator for covalent immobilization of biomolecules [19]. The optimum concentration of antibodies was determined by varying the concentration from 2 to 14 μg mL^{-1} using EIS analysis [see ESM Fig. S4(c)]. Ten micrograms per milliliter (optimized concentration) of anti-AFB_1 was uniformly immobilized onto GQDs/ITO electrodes and kept in the incubated humid chamber (25 °C) for overnight. Covalent amide bond (CO–NH) formation takes place between COOH groups of GQDs and NH_2 groups of antibodies. Finally, the immobilized electrode was treated with BSA to block non-active sites on the electrode [19]. Immobilized BSA/anti-AFB_1/GQDs/ITO glass electrode was stored at 4 °C, when not in use.

Preparation of real samples

The contaminated maize sample solutions were prepared using the earlier reported method [20]. Typically, 1 g of maize was accurately weighted from maize samples in a centrifuge tube and mixed with 20 mL of methanol/water (8:2 *v*/*v*) and 1 g NaCl. The mixture was shaken on a vortex mixer for 30 min and centrifuged at 2800*g* for 15 min. The resultant supernatant was collected and several dilutions prepared using PBS (pH 7.4). Further, different prepared dilutions were tested against bioelectrode BSA/anti-AFB_1/GQDs/ITO in PBS (0.9% NaCl) containing 5 mM $[Fe(CN)_6]^{3-/4-}$ using the EIS technique.

Results and discussion

Structural studies

Optical properties of GQDs were characterized using UV-visible spectroscopy [see ESM Fig. S1 (a)]. The UV-visible spectrum of GQDs exhibited two absorption peaks at 295 nm and 338 nm respectively. The absorption peak at 295 nm was attributed to π–π* transition due to aromatic –C=C bonds in GQDs and the absorption peak occurred at 338 nm was assigned to *n*–π* transition due to the presence of –C=O groups moiety. The radius of GQDs was calculated by using an effective mass approximation model [Eq. (1)] [21],

$$\Delta E_R = \frac{h^2\pi^2}{2R^2}\left(\frac{1}{m_e}+\frac{1}{m_h}\right)-\frac{1.8e^2}{\epsilon R} \quad (1)$$

where ΔEg is the bandgap energy (eV), ϵ is the relative dielectric constant (ϵ 5.7), $\hbar$ is the planks constant (6.626×10^{-34} J s), $m_e = 0.19m_o$, $m_h = 0.8m_o$ is the effective mass of electron and holes respectively. The radius was found to be 7 nm, and direct band gap was 3.6 eV and 4.12 eV.

An XRD technique was used to examine the crystallite size of GQDs. As shown in ESM Fig. S1 (b), the primary diffraction peak (002) observed at 2θ–23.24° found to be lower than the graphite diffraction peak value 2θ–25° confirmed the formation of GQDs. The interlayer spacing of crystallographic planes (002) found to be 0.51 nm which is higher than graphite interlayer spacing. Thus, increased spacing between the layers indicates the presence of functional groups [22]. The average crystallite size of the GQDs was calculated using the Debye-Scherrer equation [Eq. (2)] [23],

$$D = \frac{K\lambda}{\beta cos\theta} \quad (2)$$

where D is the average nanocrystal size, K is the shape factor, λ is the wavelength (0.154 nm), θ is the diffraction angle, and β is the full-width half maximum (FWHM) of the diffraction peak. The average crystallite size of GQDs found to be 7 nm.

The PL spectrum of a uniformly dispersed aqueous solution of GQDs was recorded at 365 nm and 375 nm excitation wavelength as shown in ESM Fig. S2 (a). The GQDs show prominent PL emission peak at 460 nm by exciting the photons at 375 nm, and inset images show the PL emission spectrum of GQDs at 430 nm by excitation wavelength at 365 nm. Moreover, synthesized GQDs shows the yellow color appearance under visible light and fluorescence green color emission under a source of UV lamp 365 nm wavelength [see ESM, inset image Fig. S2(a)]. Typically, the green color emission from GQDs was assigned to the functional groups and edge effects. However, ESM Fig. S2(b) shows broad PL spectra with redshifting in the emission peaks from 460 to 542 nm along with decreasing their peak of intensity where the excitation wavelength increases from 375 nm to 450 nm. The excitation-dependent PL behavior indicates the inhomogeneous orbital energy distribution of the defect states as well as it attributed to the presence of polyaromatic sp^2 carbon domains with various functional groups or moieties in the structure of GQDs [24, 25].

ESM Fig. S2(c) demonstrates the result of the Raman spectroscopy study of GQDs. The two broad peaks appeared at

1462 cm^{-1} and 1559 cm^{-1} corresponding to D-band and G-band respectively. The crystalline G-band peak and the amorphous D-band peak appeared due to the presence of aromatic domains of the E_{2g} vibrational mode in a hexagonal lattice structure [22]. Moreover, the D-band and G-band peaks originating from the disorder band caused by graphitic edges due to the sp^2/sp^3 domains and in-phase vibration of the graphite lattice. The ratio of the intensities D- and G-band "I_D/I_G" was found to be 0.97 which is higher than graphite [22]. These results indicate the presence of oxygen functional groups in the graphitic structure of nanomaterials.

The TEM studies were carried out for the structural investigation of synthesized GQDs as shown in Fig. 2a, b. The dispersed solution of GQDs for TEM analysis was prepared in distilled water, followed by ultrasonication for 30 min, then drop cast onto copper grids (3.05 mm) and dried at room temperature. Due to the presence of conducive functional groups in GQDs, their dispersion ability in aqueous solution was improved. TEM images of GQDs indicate the average size varies from 5 to 9 nm which was consistent with the results of XRD. The TEM studies revealed that GQDs are spherical, having an average crystalline size with well-ordered orientation. The lattice fringes with the interplanar distance between the two adjacent lines were found to be 0.36 nm [inset image Fig. 2b].

Morphology studies

Morphology studies of GQDs/ITO electrode and anti-AFB_1/GQDs/ITO bioelectrode were carried out using the SEM technique to investigate the changes occuring on their surface morphology. Fig. 2c, d displays synthesized GQDs are spherical in shape with uniform distribution onto ITO electrodes. After the immobilization of antibodies onto deposited electrode [Fig. 2e], the surface morphology was found to be changed from spherical to a globular structure which indicates that antibodies were successfully immobilized over the surface of the electrode.

Spectroscopy studies

Figure 3 demonstrated the FT-IR spectra of GQDs and immobilized anti-AFB_1 onto GQDs/ITO electrode. The FT-IR spectra of GQDs/ITO electrode [Fig. 3 curve (a)]

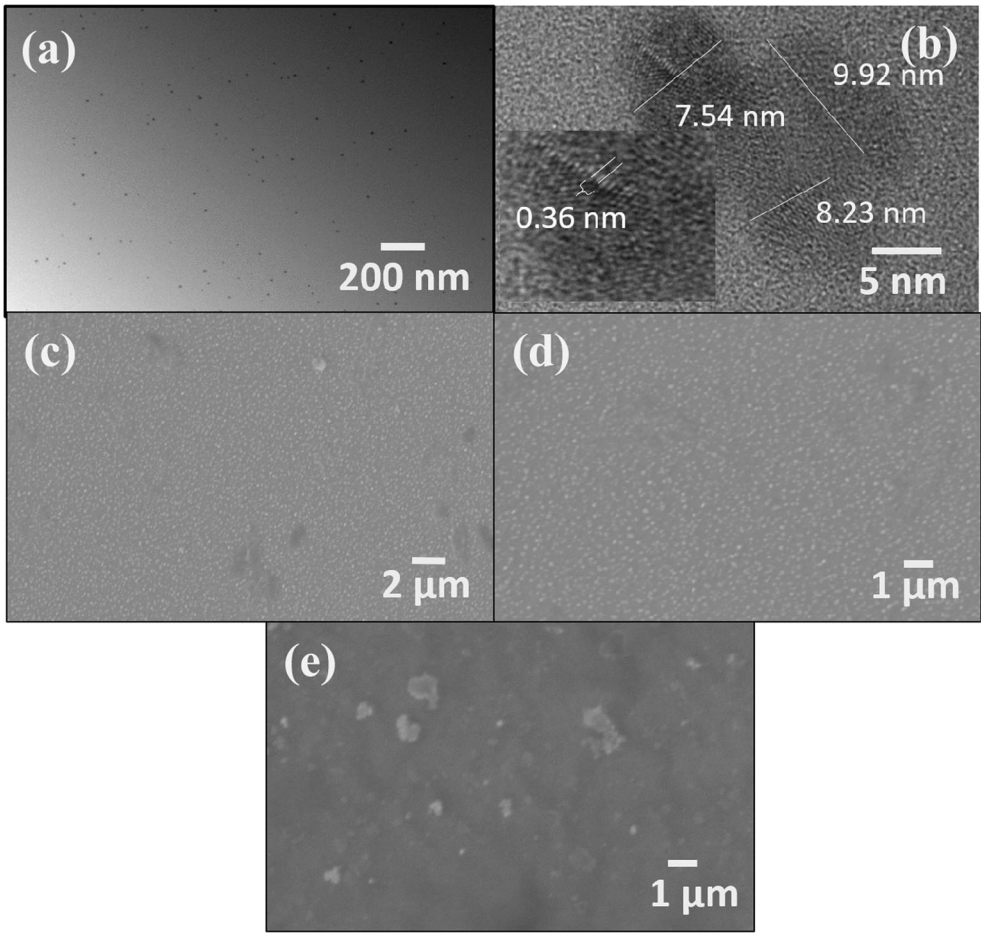

Fig. 2 TEM images of (a, b) GQDs at 200-nm scale and 5-nm scale and SEM images of GQDs/ITO deposited electrode (c, d) at 2-µm and 1-µm scale and (e) anti-AFB_1/GQDs/ITO bioelectrode at 1-µm scale

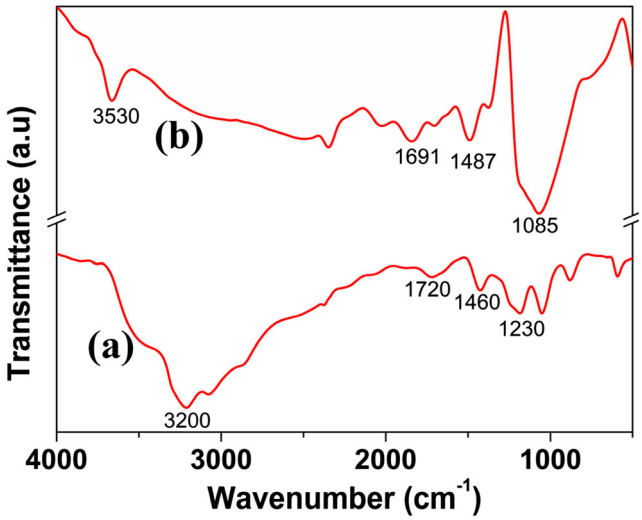

Fig. 3 FT-IR spectrum of (a) GQDs/ITO electrode and (b) anti-AFB_1/GQDs/ITO bioelectrode

show an intense peak at 3200 cm^{-1} attributed to the presence of −OH stretching vibrations in a carboxylic acid (−COOH). The peak observed at 1460 cm^{-1} and 1720 cm^{-1} corresponding to −C=C and −C=O groups, respectively, arise due to the presence of carbonyl groups and −C=C bond in GQDs. The peak observed at 1230 cm^{-1} assigned to the availability of −C−O group moiety in the GQDs. As shown in Fig. 3 curve (b), FT-IR spectra of anti-AFB_1/GQDs/ITO bioelectrode, additional two broad peaks appeared at 3530 cm^{-1} and 1487 cm^{-1} indicates the presence of −N−H groups as amide I and amide II respectively, which confirmed the immobilization of antibody onto GQDs electrode. Moreover, the peak observed at 1691 cm^{-1} corresponds to −C−O groups present in GQDs and the peak observed at 1085 cm^{-1} assigned to the C−N stretching bond of amine group that confirmed the formation of covalent bonds between −COOH groups in GQDs with $-NH_2$ groups of antibodies.

Electrochemical analysis

CV and EIS studies were conducted using GQDs/ITO electrode, anti-AFB_1/GQDs/ITO and BSA/anti-AFB_1/GQDs/ITO bioelectrodes in 50 mM PBS containing (0.9% NaCl) 5 mM $[Fe(CN)_6]^{3-/4-}$ as a redox species at pH 7.4.

Cyclic voltammetry studies

The CV analysis of the electrodes GQDs/ITO, anti-AFB_1/GQDs/ITO, and BSA/anti-AFB_1/GQDs/ITO were carried out at scan rate of 50 mV s^{-1} with an applied potential range from − 0.7 V to +0.7 V [see ESM Fig. S3(a)]. The magnitude of the anodic and cathodic peak current of GQDs/ITO electrode was found to be 458.3 μA and − 376.4 μA respectively. Similarly, oxidation and reduction peak current of bioelectrodes anti-AFB_1/GQDs/ITO and BSA/anti-AFB_1/GQDs/ITO were found to be 417.8 μA, − 335.4 μA and 399.82 μA, and − 353.24 μA respectively. The oxidation peak potential of the GQDs/ITO electrode was found to be slightly higher (0.29 V) in comparison to the anti-AFB_1/GQDs/ITO (0.28 V) and BSA/anti-AFB_1/GQDs/ITO bioelectrodes (0.27 V). The GQDs/ITO electrode shows higher current as compared to immobilized electrodes because of the electron detaching behavior of GQDs. After the immobilization of anti-AFB_1 onto the deposited electrode, the current value was found to be decreased, probably by an insulating behavior of anti-AFB_1 that hindered the transfer of electrons towards the electrode surface. The current response was further reduced when the electrode was treated with BSA because BSA blocks the non-specific active sites [26].

The surface concentration of BSA/anti-AFB_1/GQDs/ITO and anti-AFB_1/GQDs/ITO bioelectrodes were estimated to be 1.69×10^{-8} mol cm^{-2} and 1.78×10^{-8} mol cm^{-2} whereas the surface concentration of GQDs/ITO-deposited electrode was found to be 1.94×10^{-8} mol cm^{-2} that confirmed immobilization of anti-AFB_1 onto the deposited electrode surface. The surface concentration of the electrode matrix was calculated by the Brown-Anson model [Eq. (3)] [27],

$$I_P = \frac{n^2 F^2 I^* A V}{4RT} \tag{3}$$

where *I*p is the peak current (μA), *A* is the area of the electrode (cm^2), *V* is the scan rate (V s^{-1}), *R* is the gas constant (J K^{-1} mol^{-1}), *T* is the temperature (K), *F* is the Faraday constant (C mol^{-1}), and *I** is the surface concentration of the electroactive species (mol cm^{-2}).

CV studies were carried out using bioelectrode BSA/anti-AFB_1/GQDs/ITO as a function of scan rate from 10 to 300 mV s^{-1} [see ESM Fig. S3(b)]. The anodic peaks were observed to be increased towards the positive potential, and cathodic peaks were shifted towards the negative potential by increasing the scan rate resulted as a diffusion-controlled process for the redox reaction [27]. The anodic and cathodic peak current and potential vary proportionally with the square root of scan rate Eqs. (4–7).

$$I_{ac} = 67.86\ \mu A + 47.86\ \left(\mu A^2\ m\ V^{-1}\ s\right)^{1/2} \times \left[scan\ rate\ \left(mV\ s^{-1}\right)\right]^{1/2}; R^2 = 0.99 \tag{4}$$

$$I_{cc} = -130.47\ \mu A - 27.94\ \left(\mu A^2\ m\ V^{-1}\ s\right)^{1/2} \times \left[scan\ rate\ \left(mV\ s^{-1}\right)\right]^{1/2}; R^2 = 0.99 \quad (5)$$

$$V_{ap} = 2.0 \times 10^{-1}\ (V) + 1.6 \times 10^{-2}\ (V) \times \left[scan\ rate\ \left(mV\ s^{-1}\right)\right]^{1/2}; R^2 = 0.99 \quad (6)$$

$$V_{cp} = 1.2 \times 10^{-1}\ (V) - 1.6 \times 10^{-2}\ (V) \times \left[scan\ rate\ \left(mV\ s^{-1}\right)\right]^{1/2}; R^2 = 0.98 \quad (7)$$

where, I_{ac} and I_{cc} anodic and cathodic peak current and V_{ap} and V_{cp} are the anodic and cathodic peak potential respectively.

However, the diffusion coefficient was estimated to be 7.0×10^{-6} cm^2 s^{-1} for BSA/anti-AFB_1/GQDs, calculated by Randles-Sevcik equation [Eq. 8] [28],

$$I_P = 2.69x10^5 n^{\frac{3}{2}} A D^{\frac{1}{2}} V^{\frac{1}{2}} C \quad (8)$$

where I_p is the peak current of bioelectrode, n is the number of electrons involved in the process, C is the concentration of redox species 5 mM $[Fe(CN)_6]^{3-/4-}$, D is the diffusion coefficient, v is the scan rate (50 mV s^{-1}).

Electrochemical impedance spectroscopy studies

EIS is a non-destructive, versatile, and powerful as well as label-free technique (without any targeted reagents) that may yield rapid, simple, and low-cost detection due to complex resistance and capacitance changes occurring on the electrode and electrolyte interfaces [28]. The EIS technique is used to determine the complex electrical impedance signal of an electrochemical system occurred at the interface between the surface of the electrode and electrolyte solution. The electrochemical impedance behavior can be determined by applying a small amount of voltage; accordingly, it measures the impedance response as a Nyquist plot (combination of real and imaginary part of impedance) with the function of frequency [28]. The Randel's equivalent circuit is one of the most common model which includes solution resistance (R_s), double-layer capacitance (C_{dl}), charge transfer resistance (polarization resistance R_{CT}), and Warburg impedance (diffusion of ions at the interface of the electrode surface and an electrolyte solution in electrochemical system). In the Nyquist plot, R_{CT} behavior of an electrode was presented by a semicircle diameter forming at the higher frequency region corresponding to an electron-limiting process whereas a diffusion-controlled process exhibited at the lower frequency region. Figure 4(a) shows the results of EIS spectra of (a) GQDs/ITO, (b) anti-AFB_1/GQDs/ITO, and (c) BSA/anti-AFB_1/GQDs/ITO electrodes in PBS (pH 7.4) containing 5 mM $[Fe(CN)_6]^{3-/4-}$, as a function of frequency range (0.01–100 kHz) at a bias potential of 0.25 V. The R_{CT} value of GQDs/ITO electrode was found to be 109 Ω because of the electrophoretic deposit of GQDs onto the surface matrix resulting in an enhancement of the electron transfer phenomenon. After the immobilization of antibody onto an electrode surface of anti-AFB_1/GQDs/ITO, R_{CT} value found to be 246 Ω which was higher than GQDs/ITO electrode R_{CT} value. This increase in the R_{CT} value indicates conjugation of biomolecules with nanomaterials GQDs. Further, the bioelectrode treated with BSA, R_{CT} value found to be increased up to 257 Ω because BSA blocks the non-active sites on the electrode surface. To figure out the specificity of the antigen AFB_1, a control experiment was carried out using the GQDs/ITO electrode treated with BSA (1 mg mL^{-1}). This fabricated electrode was tested against the different concentration of antigen AFB_1 range varying from 0.1 to 2.0 ng mL^{-1}. There were no significant changes observed in the R_{CT} value indicating the antigen is highly specific for the antibody [see ESM Fig. S4 (a)]. The electron transfer kinetics of the redox probe occurred at the electrode/electrolyte interface varied through modifying the electrode matrix. Any insulating modification on the electrode is expected to retard the interfacial electron transfer kinetics, thereby enhancing the electron transfer resistance. Further, bioelectrode characterized by evaluating the various important parameters such as heterogenous electron transfer (HET) and time constant for the redox probe. These important parameters not only allow knowing the interfacial interaction of the structural features of the sensing interface but also explain the mechanisms of the chemical process occurring at the electrode/electrolyte interface. The change in the HET value indicated about the speed of electron exchange between the redox probe and electrode matrix. The HET of the electrodes GQDs/ITO, anti-AFB_1/GQDs/ITO, and BSA/anti-AFB_1/GQDs/ITO was calculated using Eq. (9) [29],

$$K_e = \frac{RT}{n^2 F^2 A R_{CT} C} \quad (9)$$

where, R is the gas constant (J K^{-1} mol^{-1}), T is the temperature (K), n is the number of electrons transfer, F is the Faraday constant (C mol^{-1}), A is the effective area of electrode (cm^2), R_{CT} is the charge transfer resistance (Ω), and C is the concentration of redox species in the bulk solution (mol cm^{-3}). The K_e value of electrode GQDs/ITO was found to be 97.63×10^{-5} cm s^{-1} whereas K_e value of the bioelectrodes BSA/anti-AFB_1/GQDs/ITO and anti-AFB_1/

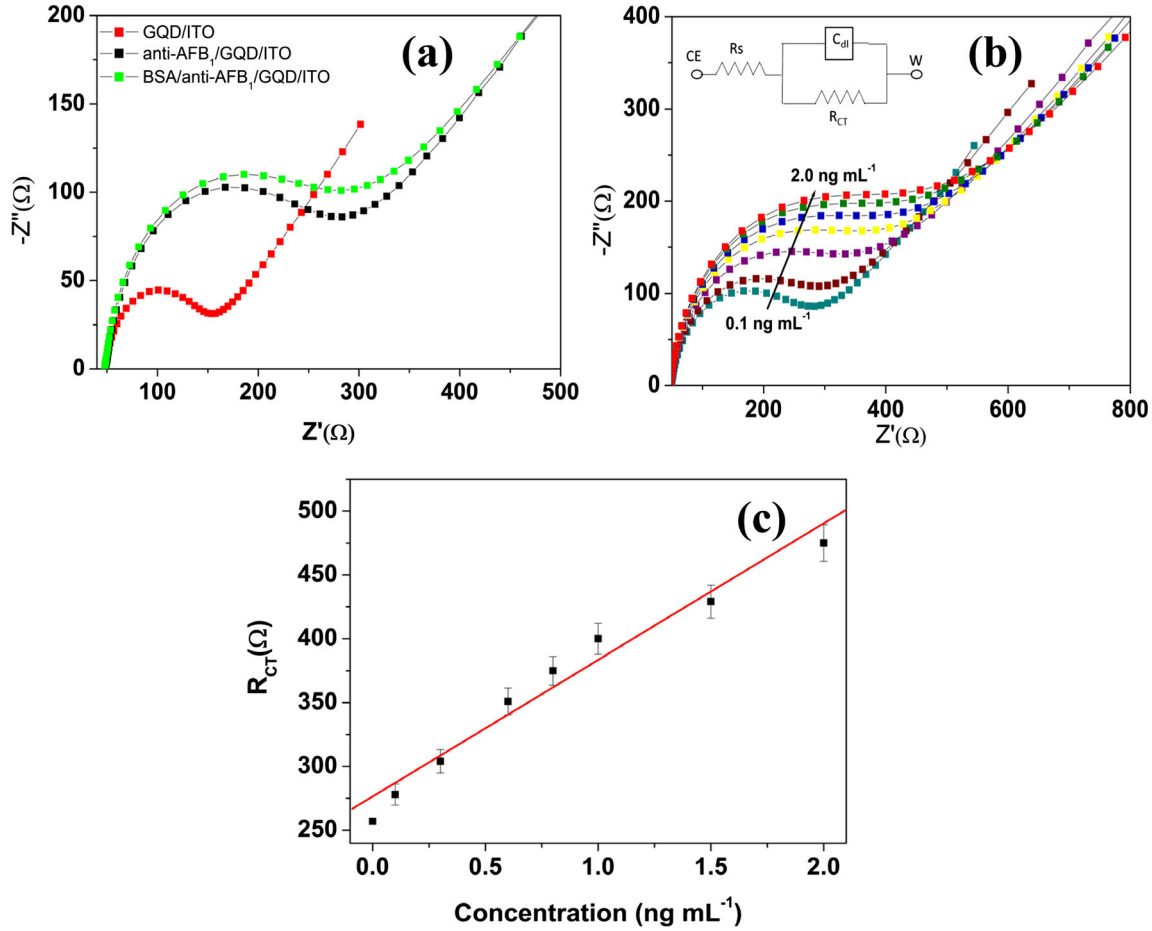

Fig. 4 (a) EIS spectrum of GQDs/ITO, anti-AFB_1/GQDs/ITO, BSA/anti-AFB_1/GQDs/ITO electrode in PBS (pH 7.4) containing 5 mM $[Fe(CN)_6]^{3-/4-}$, (b) EIS response of BSA/anti-AFB_1/GQDs/ITO bioelectrode for varying concentration of AFB_1 (0.1–2.0 ng mL^{-1}) in PBS (pH 7.4) containing 5 mM $[Fe(CN)_6]^{3-/4-}$[Inset image shows the Randles equivalent circuit, and (c) calibration plot showing the variation in charge transfer resistance (R_{CT}) with AFB_1 concentration (0.1–2.0 ng mL^{-1})

GQDs/ITO were found to be 41.40 × 10^{-5} cm s^{-1} and 41.74 × 10^{-5} cm s^{-1}. It has been noticed that decreased in the K_e value with bioelectrode revealed about decreased in the electron transfer kinetics due to higher loading of anti-AFB_1 onto the deposited electrode. Moreover, we have calculated the various parameters of electrodes depicted in [see ESM Table S2]. And, in this study another important parameter is calculated as the time constant (tau) value for the corresponding charge transfer process. The time constant value determined by the maximum frequency ($\omega = 2\pi f$), in which semicircle draws a maximum in the imaginary axis using Eq. (10),

$$\tau = 1/\omega\_max = R\_CT\ C\_dl \tag{10}$$

The tau value of the electrodes GQDs/ITO, anti-AFB_1/GQDs/ITO, and BSA/anti-AFB_1/GQDs/ITO were found to be 0.005 s, 0.012 s, and 0.014 s. The tau value of GQDs/ITO electrode was found to be lowest at 0.005 s due to the faster reaction taking place in the redox electrolyte species, whereas the tau value found to be increased after immobilization of antibody onto deposited electrode, resulting in slower diffusion of $[Fe(CN)_6]^{3-/4-}$ ions in the electrochemical process.

Electrochemical response studies

The electrochemical immunosensing response of the bioelectrode BSA/anti-AFB_1/GQDs/ITO was conducted with the function of antigen concentration 0.1–2.0 ng mL^{-1} as shown in Fig. 4b. In the Nyquist plot, the diameter of the semicircle increased as the concentration of antigen AFB_1 increased, resulting in antigen AFB_1 interacting with the anti-AFB_1 by immunocomplex formation. Increasing the concentration of AFB_1 resulted in more accumulation of the antigen-antibody complex at the sensor surface leading to enhanced electrochemical impedance signal. On further addition of AFB_1 in the electrolyte redox probe PBS containing 5 mM $[Fe(CN)_6]^{3-/4-}$, therewas no further increment in the R_{CT} value [see ESM Fig. S4 (d)]. This indicates that there were no remaining antibodies available onto the electrode surface which

may interact with more antigens; this revealed that the specific available sites of the antibodies get saturated. The calibration curve between R_{CT} value and concentration of AFB_1 is depicted in Fig. 4c. It has been shown that this immunoelectrode BSA/anti-AFB_1/GQDs/ITO has a linear detection range from 0.1 to 2.0 ng mL^{-1}. The sensitivity of the immunoelectrode was found to be (213.88 Ω (ng mL^{-1})$^{-1}$ cm^{-2}.

$$R_{CT(\Omega)} = 276.493\ \Omega + 106.9443\left(\Omega\ ng^{-1}\ mL\right)x0.3\ ng\ mL^{-1} \tag{11}$$

The high sensitivity of the immunoelectrode BSA/anti-AFB_1/GQDs/ITO may assign to the presence of oxygen-containing groups in GQDs which have strong capability to adsorb the biomolecules covalently. The nanocrystal size of GQDs attributed to the enhancement of the surface concentration of the electrode. In comparison to the other matrices, GQDs-based platform provides the linear sensing detection range is from 0.1–2.0 ng mL^{-1} along with high sensitivity. The smart material GQDs improve the biosensing characteristics along with some important parameters of the biosensor as HET characteristics and time constant. The specific characteristic and functional parameters of the currently designed immunosensor were found to be better as compared to previously reported. For example, Beizaei et al. demonstrate the highly sensitive toxic microarray for AFB_1 detection and limit of detection found to be 1 pg g^{-1} [30]. Moreover, Liu et al. developed the novel monoclonal antibodies-based ultrasensitive ELISA for AFB_1 detection with a detection limit of immunostrip at 1.0 ng mL^{-1} [31]. The lower detection limit was calculated by (Eq. 12) [32],

$$\text{Detection limit} = \frac{3\sigma}{m} \tag{12}$$

where σ is the standard deviation and m is the slope. The fabricated immunosensor could be able to detect up to the lowest concentration (0.03 ng mL^{-1}) of AFB_1 in food compared to the other reported biosensors. The three-dimensional structure of GQDs act as a significant nanomaterial owing to the availability of conducive functional groups which have been utilized for covalent binding of specific antibodies of AFB_1 using crosslinker leading to the improvement of their chemisorption phenomenon, electron transfer efficacy, stability, and conductivity of electrochemical biosensor. Moreover, a control experiment was performed using the electrode GQDs/ITO in PBS containing $[Fe(CN)_6]^{3-/4-}$ by varying the antigen concentration from (0.1–2.0 ng mL^{-1}) using the EIS technique to check out the antibody-antigen interactions [see ESM Fig. S4(b)]. We noticed that no significant change had been observed in the R_{CT} value, indicating that AFB_1 was highly selective for the anti-AFB_1.

Reproducibility and stability studies

The reproducibility studies of immunosensor were carried out by using seven different electrodes under the same set of experimental conditions with a concentration of antigen AFB_1 (0.1 ng mL^{-1}). It was observed that there was a negligible modulation in R_{CT} value. The relative standard deviation (RSD) value was found to be 1.71% with a respective mean value of 262.4 [Fig. 5a]. This indicates that the electrochemical immunosensor for AFB_1 is reproducible. The stability studies of the immunoelectrode were carried out using the EIS technique. As shown in Fig. 5b, the EIS response of the bioelectrode BSA/anti-AFB_1/GQDs/ITO recorded as a function of a number of days in the interval of 1 week up to 8 consecutive weeks. It was found that there was negligible variation in the R_{CT} value from the observed initial value up to 7 weeks. Thus, these bioelectrodes retain their activity up to

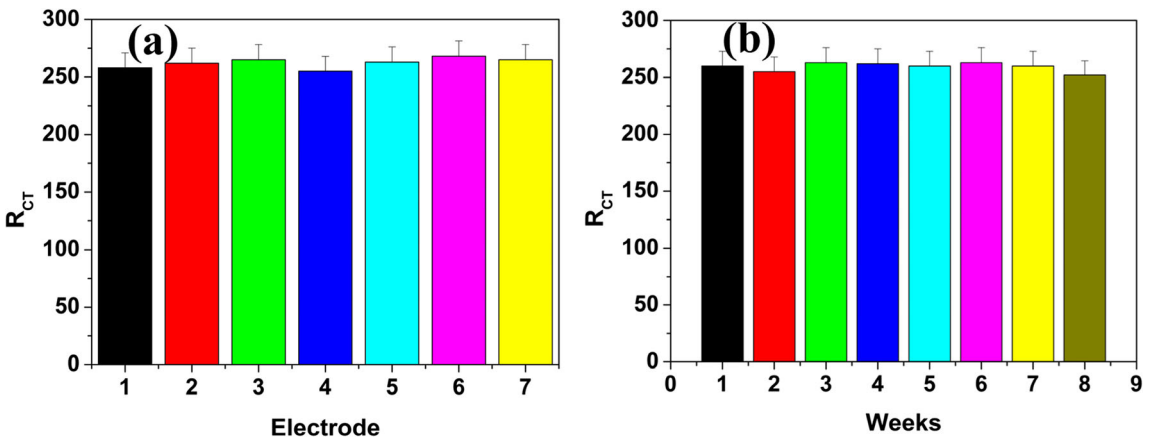

Fig. 5 (a) The EIS response of seven different bioelectrodes BSA/anti-AFB_1/GQDs/ITO were studied in the presence of AFB_1 concentration 0.1 ng mL^{-1} in PBS (pH 7.4) containing 5 mM $[Fe(CN)_6]^{3-/4-}$ and (b) the EIS response of BSA/anti-AFB_1/GQDs/ITO bioelectrode as a function of weeks

7 weeks by decreasing only 2–5%, but after that, the bioelectrode shows a significant decrease in their activity due to degradation of biomolecules. The stability of the immunoelectrode may be assigned to the covalent interactions of the antibody with the deposited nanomaterials.

In the literature, several methods were reported for the detection of AFB_1. A comparative report of this fabricated BSA/anti-AFB_1/GQDs/ITO immunosensor with other published works is shown in ESM Tables S1[33–40] and S3[41–44, 46, 47] for the detection of AFB_1 in foodstuffs and feeds. In the present study, we found better results as compared to previously reported results. The electrochemical immunosensor using GQDs-based platform shows several advantages such as high surface to volume ratio, excellent biocompatibility, abundant hydrophilic edges and hydrophobic planes that favors the antibody adsorption over the electrode surface, enhances the electron transfer phenomenon, electrode/ion conduction with shorter electron transportation and diffusion length for ion transport. Thus, biosensing sensing performance regarding sensitivity, detection limit, specificity, and reproducibility for AFB_1 detection has been achieved better which act as a novel electrode in the field of electrochemical biosensing.

Real sample analysis

Contaminated maize samples were procured from the Indian Agricultural Research Institute (IARI), New Delhi, India. The different concentration of AFB_1 samples was prepared in PBS solution and tested against bioelectrode BSA/anti-AFB_1/GQDs/ITO in PBS (pH 7.4) containing 5 mM $[Fe(CN)_6]^{3-/4-}$ using EIS technique and the obtained results were shown in ESM Fig. S5(a, b). The impedance response of the bioelectrode increases by increasing the concentration of AFB_1 from (0.1–1.75 ng mL^{-1}). The regression coefficient found to be 0.98 revealed that there is a high correlation between impedance response and concentration. The LOD was found to be 0.05 ng g^{-1}. Therefore, it is a very simple, rapid, and reliable technique for the detection of AFB_1 in food contents and feeds.

Conclusions

In summary, we designed a label-free electrochemical immunosensor based on the GQDs platform for the detection of aflatoxin B_1 in food contents and feeds. Chemically synthesized GQDs deposited onto ITO-coated glass substrates using the EPD technique where the deposited electrode has –COOH groups which are being utilized to conjugate the anti-AFB_1 having NH_2 groups via covalent amide bonding linkage (CO–NH). Thus, large surface area, good conductivity, ease of electron transfer efficacy, low toxicity, biocompatibility of GQDs-based platform provide selective, specific, and reproducible immunoassay. The proposed electrochemical immunosensor exhibits a wide range of detection (0.1–2.0 ng mL^{-1}), high sensitivity 213.888 Ω (ng $mL^{-1})^{-1}$ cm^{-2}, and an improved detection limit (0.03 ng mL^{-1}). This biosensor served for better reproducibility and storage stability up to 7 weeks. The fabricated immunosensor utilized for real sample analysis as maize food product resulting detection limit found to be 0.05 ng g^{-1}, indicating its potential application as rapid detection of AFB_1 in food contents.

Acknowledgements The authors are highly thankful to Director, CSIR-National Physical Laboratory, New Delhi, India, for providing the facilities. We thank Dr. A.M. Biradar for his support and encouragement. The authors are thankful to Prof. B. D. Malhotra, Delhi Technical University, for his guidance and useful discussions. H.B. acknowledges the Department of Science and Technology (DST) for financial support, Dr. Ritu Srivastava for PL studies, Mr. Manoj Kumar Pandey for technical help, and Mrs. Monika Kundu for providing infected maize samples. C.S. acknowledges CSIR (India), for the award of Senior Research Fellowship. Authors are also thankful to Mr. Dinesh Singh and Mr. K. N. Sood for TEM and SEM studies.

Compliance with ethical standards

Conflict of interest The authors declare that they have no conflict of interest.

References

1. Conradt D, Schatzle MA, Haas J, Townsend CA, Muller M. New insights into the conversion of Versicolorin a in the biosynthesis of aflatoxin B1. J Am Chem Soc. 2015;137(34):10867–9.
2. Wang X, Niessner R, Tang D, Knopp D. Nanoparticle-based immunosensors and immunoassays for aflatoxins. Anal Chim Acta. 2016;912:10–23.
3. Parkin DM, Bray F, Ferlay J, Pisani P. Estimating the world cancer burden: Globocan 2000. Int J Cancer. 2001;94(2):153–6.
4. Van Egmond HP, Schothorst RC, Jonker MA. Regulations relating to mycotoxins in food. Anal Bioanal Chem. 2007;389(1):147–57.
5. Ketney O, Santini A, Oancea S (2017) Recent aflatoxin survey data in milk and milk products: A review. Int J Dairy Technol.
6. Suzuki N, Wang Y, Elvati P, Qu Z-B, Kim K, Jiang S, et al. Chiral graphene quantum dots. ACS Nano. 2016;10(2):1744–55.
7. Wang J. Nanomaterial-based electrochemical biosensors. Analyst. 2005;130(4):421–6.
8. Shen J, Zhu Y, Yang X, Li C. Graphene quantum dots: emergent nanolights for bioimaging, sensors, catalysis and photovoltaic devices. Chem Commun. 2012;48(31):3686–99.
9. Zhang P, Zhuo Y, Chang Y, Yuan R, Chai Y. Electrochemiluminescent graphene quantum dots as a sensing platform: a dual amplification for microRNA assay. Anal Chem. 2015;87(20):10385–91.
10. Yang H, Liu W, Ma C, Zhang Y, Wang X, Yu J, et al. Gold-silver nanocomposite-functionalized graphene based electrochemiluminescence immunosensor using graphene quantum dots coated porous PtPd nanochains as labels. Electrochim Acta. 2014;123:470–6.
11. Ren M, Xu H, Huang X, Kuang M, Xiong Y, Xu H, et al. Immunochromatographic assay for ultrasensitive detection of

aflatoxin B1 in maize by highly luminescent quantum dot beads. ACS Appl Mater Interfaces. 2014;6(16):14215–22.
12. Qian ZS, Shan XY, Chai LJ, Ma JJ, Chen JR, Feng H. DNA nanosensor based on biocompatible graphene quantum dots and carbon nanotubes. Biosens Bioelectron. 2014;60:64–70.
13. Zhang Y, Wu C, Zhou X, Wu X, Yang Y, Wu H, et al. Graphene quantum dots/gold electrode and its application in living cell H 2 O 2 detection. Nanoscale. 2013;5(5):1816–9.
14. Deng L, Liu L, Zhu C, Li D, Dong S. Hybrid gold nanocube@ silica@ graphene-quantum-dot superstructures: synthesis and specific cell surface protein imaging applications. Chem Commun. 2013;49(25):2503–5.
15. Xie R, Wang Z, Zhou W, Liu Y, Fan L, Li Y, et al. Graphene quantum dots as smart probes for biosensing. Anal Methods. 2016;8(20):4001–16.
16. Dikin DA, Stankovich S, Zimney EJ, Piner RD, Dommett GHB, Evmenenko G, et al. Preparation and characterization of graphene oxide paper. Nature. 2007;448(7152):457–60.
17. Pan D, Zhang J, Li Z, Wu M. Hydrothermal route for cutting graphene sheets into blue-luminescent graphene quantum dots. Adv Mater. 2010;22(6):734–8.
18. Singh C, Srivastava S, Ali MA, Gupta TK, Sumana G, Srivastava A, et al. Carboxylated multiwalled carbon nanotubes based biosensor for aflatoxin detection. Sens Actuators B: Chemical. 2013;185:258–64.
19. Bhardwaj H, Singh C, Kumar Pandey M, Sumana G. Star shaped zinc sulphide quantum dots self-assembled monolayers: preparation and applications in food toxin detection. Sens Actuators B: Chemical. 2016;231:624–33.
20. Ma H, Sun J, Zhang Y, Xia S. Disposable amperometric immunosensor for simple and sensitive determination of aflatoxin B 1 in wheat. Biochem Eng J. 2016;115:38–46.
21. Brus LE. Electron-electron and electron-hole interactions in small semiconductor crystallites: the size dependence of the lowest excited electronic state. J Chem Phys. 1984;80(9):4403–9.
22. Li L, Wu G, Yang G, Peng J, Zhao J, Zhu J-J. Focusing on luminescent graphene quantum dots: current status and future perspectives. Nanoscale. 2013;5(10):4015–39.
23. Urraca JL, Huertas-Pérez JF, Cazorla GA, Gracia-Mora J, García-Campana AM. Moreno-Bondi MaC. Development of magnetic molecularly imprinted polymers for selective extraction: determination of citrinin in rice samples by liquid chromatography with UV diode array detection. Anal Bioanal Chem. 2016;408(11):3033–42.
24. Minati L, Torrengo S, Maniglio D, Migliaresi C, Speranza G. Luminescent graphene quantum dots from oxidized multi-walled carbon nanotubes. Mater Chem Phys. 2012;137(1):12–6.
25. Wu ZL, Gao MX, Wang TT, Wan XY, Zheng LL, Huang CZ. A general quantitative pH sensor developed with dicyandiamide N-doped high quantum yield graphene quantum dots. Nanoscale. 2014;6(7):3868–74.
26. Babacan S, Pivarnik P, Letcher S, Rand AG. Evaluation of antibody immobilization methods for piezoelectric biosensor application. Biosens Bioelectron. 2000;15(11):615–21.
27. Khan R, Kaushik A, Solanki PR, Ansari AA, Pandey MK, Malhotra BD. Zinc oxide nanoparticleschitosan composite film for cholesterol biosensor. Anal Chim Acta. 2008;616(2):207–13.
28. Bard AJ, Faulkner LR, Leddy J, Zoski CG. Electrochemical methods: fundamentals and applications (vol. 2). New York: Wiley; 1980.
29. Kaushik A, Solanki PR, Kaneto K, Kim CG, Ahmad S, Malhotra BD. Nanostructured iron oxide platform for impedimetric cholesterol detection. Electroanalysis. 2010;22(10):1045–55.
30. Beizaei A, O'Kane SL, Kamkar A, Misaghi A, Henehan G, Cahill DJ. Highly sensitive toxin microarray assay for aflatoxin B1 detection in cereals. Food Control. 2015;57:210–5.
31. Liu J-W, Lu C-C, Liu B-H, Yu F-Y. Development of novel monoclonal antibodies-based ultrasensitive enzyme-linked immunosorbent assay and rapid immunochromatographic strip for aflatoxin B1 detection. Food Control. 2016;59:700–7.
32. Long GL, Winefordner JD (1983) Limit of detection. A closer look at the IUPAC definition. Anal Chem 55(7).
33. Wu S, Duan N, Zhu C, Ma X, Wang M, Wang Z. Magnetic nanobead-based immunoassay for the simultaneous detection of aflatoxin B 1 and ochratoxin a using upconversion nanoparticles as multicolor labels. Biosens Bioelectron. 2011;30(1):35–42.
34. Kalita P, Singh J, Kumar Singh M, Solanki PR, Sumana G, Malhotra BD. Ring like self assembled Ni nanoparticles based biosensor for food toxin detection. Appl Phys Lett. 2012;100(9): 093702.
35. Liu Y, Qin Z, Wu X, Jiang H. Immune-biosensor for aflatoxin B 1 based bio-electrocatalytic reaction on micro-comb electrode. Biochem Eng J. 2006;32(3):211–7.
36. Chuan Li S, Hua Chen J, Cao H, Sheng Yao D, Ling Liu D. Amperometric biosensor for aflatoxin B 1 based on aflatoxin-oxidase immobilized on multiwalled carbon nanotubes. Food Control. 2011;22(1):43–9.
37. Srivastava S, Kumar V, Ali MA, Solanki PR, Srivastava A, Sumana G, et al. Electrophoretically deposited reduced graphene oxide platform for food toxin detection. Nanoscale. 2013;5(7):3043–51.
38. Yagati AK, Chavan SG, Baek C, Lee M-H, Min J (2018) Label-free impedance sensing of aflatoxin B1 with polyaniline nanofibers/au nanoparticle electrode array. Sensors (Basel, Switzerland) 18(5).
39. Foguel MV, Furlan Giordano G, de Sylos CM, Carlos IZ, Pupim Ferreira AA, Benedetti AV, et al. A low-cost label-free AFB1 impedimetric immunosensor based on functionalized CD-trodes. Chemosensors. 2016;4(3):17.
40. Liang Y, Baker ME, Yeager BT, Denton MB. Quantitative analysis of aflatoxins by high-performance thin-layer chromatography utilizing a scientifically operated charge-coupled device detector. Anal Chem. 1996;68(22):3885–91.
41. Sun PS, Chu FS. A simple solid-phase radioimmunoassay for aflatoxin B1. J Food Saf. 1977;1(1):67–75.
42. Tan Y, Chu X, Shen G-L, Yu R-Q. A signal-amplified electrochemical immunosensor for aflatoxin B1 determination in rice. Anal Biochem. 2009;387(1):82–6.
43. Zaijun L, Zhongyun W, Xiulan S, Yinjun F, Peipei C. A sensitive and highly stable electrochemical impedance immunosensor based on the formation of silica gel-ionic liquid biocompatible film on the glassy carbon electrode for the determination of aflatoxin B1 in bee pollen. Talanta. 2010;80(5):1632–7.
44. Trucksess MW, Nesheim S, Eppley RM. Thin layer chromatographic determination of deoxynivalenol in wheat and corn. Journal-Association of Official Analytical Chemists. 1984;67(1):40–3.
45. Foguel MV, Furlan Giordano G, de Sylos CM, Carlos IZ, Pupim Ferreira AA, Benedetti AV, et al. A low-cost label-free AFB1 impedimetric immunosensor based on functionalized CD-trodes. Chemosensors. 2016;4(3):17.
46. Lin Y, Zhou Q, Tang D, Niessner R, Knopp D. Signal-on photoelectrochemical immunoassay for aflatoxin B1 based on enzymatic product-etching MnO_2 nanosheets for dissociation of carbon dots. Anal Chem. 2017;89(10):5637–45.
47. Shim W-B, Kim MJ, Mun H, Kim M-G. An aptamer-based dipstick assay for the rapid and simple detection of aflatoxin B1. Biosens Bioelectron. 2014;62:288–94.